Morphology is a Link to the Past: examining formative and secular galactic evolution through morphology

A THESIS
SUBMITTED TO THE FACULTY OF THE GRADUATE SCHOOL
OF THE UNIVERSITY OF MINNESOTA
BY

Melanie A. Galloway

IN PARTIAL FULFILLMENT OF THE REQUIREMENTS
FOR THE DEGREE OF
Doctor of Philosophy

Advisor:

Lucy Fortson

month, 2017

Acknowledgements

Some acknowledgements

Dedication

Firstly dedicated to Zuko, for being the sweetest little bird.

Abstract

Galaxy morphology is one of the primary keys to understanding a galaxy's evolutionary history. External mechanisms (environment/clustering, mergers) have a strong impact on formative evolution of the major galactic components (disk, bulge, Hubble type), while internal instabilities created by bars, spiral arms, or other substructures drive secular evolution via the rearrangement of material within the disk. This thesis will explore several ways in which morphology may impact the dynamics and evolution of a galaxy using visual classifications from several Galaxy Zoo projects. Section 1 will focus on the present morphology of galaxies in the local Universe ($z < 0.2$) using data from Galaxy Zoo 2 and Galaxy Zoo UKIDSS. Section 2 will examine populations of morphologies at various lookback times, from $z = 0$ out to $z = 1$ using data from Galaxy Zoo Hubble.

We first explore the impact of bars in disc galaxies on channeling gas from the outer regions of the disk to the inner few kpc necessary to fuel an active galactice nucleus (AGN). Using a sample of 19,756 disk galaxies at $0.01 < z < 0.05$ imaged by the Sloan Digital Sky Survey and morphologically classified by Galaxy Zoo 2, the difference in AGN fraction in barred and unbarred disks was measured. A weak, but statistically significant, effect was found in that the population of AGN hosts exhibited a 16.0% increase in bar fraction as compared to their unbarred counterparts at fixed mass and color. These results are consistent with a cosmological model in which bar-driving fueling contributes to the fueling of growing black holes, but other dynamical mechanisms must also play a significant role.

We study the wavelength dependence on morphology by comparing the optical morphological classifications from GZ2 to classifications done on infrared images in GZ:UKIDSS. We find some cool result. [to be continued]

We examine more directly the morphological changes in galaxy populations as a function of their age using classifications from Galaxy Zoo: Hubble. A sample of XX,XXX disc galaxies from the COSMOS field at $0 < z < 1$ were identified as active or passive using a NUV-r / r -J diagnostic with rest-frame colors from the UltraVISTA catalog. We find that the fraction of disks that are passive increases/decreases from X.X% at

$z = 1$ to X.X% at $z = 0$. We intepret this result as [something having to do with the transformation of disk to elliptical, depending on result]. Addionally, we emphasize the challenges of visual classification that are particular to galaxies at high redshift. We present a correction technique to address these biases using simulated images of nearby SDSS galaxies which were artificially redshifted using the FERENGI code and classified in GZH.

Contents

List of Tables

List of Figures

Chapter 1

Introduction

The Intro

Chapter 2

Bar AGN project

Basically Galloway et al. 2015 Muzahid et al. (2015)

Chapter 3

UKIDSS

UKIDSS science and debiasing.

Chapter 4

Using FERENGI to correct f_{features} for redshift-induced classification bias

4.1 Intro

The GZ vote fraction f_{features} plays a crucial role in the majority of science cases that use Galaxy Zoo classifications. It represents the fraction of users who answered "feature or disk" to the first question in the decision tree, and is used to distinguish elliptical/spheroidal galaxies from those with features. Many studies aim to measure the popluation of galaxies exhibiting certain features such as bars (examples), spiral arms (examples), [dump stuff in this list]. In each of these, f_{features} is necessary for creating the sample of galaxies which could potentially contain the feature in question. This is typically acheived by setting a cut, such that all galaxies with f_{features} greater than that threshold are considered to be candidates for that study.

While f_{features} is not a true probability, the measurement is intended to be consistent among all galaxies; that is, two galaxies with similar f_{features} values should have similar likelihoods of being featured (or not featured). This has been shown to be true at low redshift by comparing the f_{features} values to expert classifications (reference Willet et al. 2013); there is a strong correlation between this vote fraction and whether the galaxy

was expertly classified as a disk or an elliptical [expand on what W13 actually did.].

For distant galaxies, however, we observe that f_{features} is not consistant with nearby galaxies. As galaxies are observed at higher redshift, the images are inherently less resolved, and smaller features are more difficult to identify. This causes in a decrease in f_{features} than what would be expected if the galaxy had been observed at $z = 0$. Figure [make a figure] shows this effect: [describe some figure, probably a bunch of galaxies that are obviously spirals but with very diff. ffeatures values at diff. redshifts.] Therefore, two identical galaxies, imaged at different redshift, may have small to drastic differences in their f_{features} measurement. In order to keep f_{features} a value correlated with the likelihood of having features that is consistent for *all* galaxies, this bias must be corrected.

A method for correcting redshift bias in the GZ vote fractions was developed and implemented in prior Galaxy Zoo projects (cite GZ1 and GZ2), which contained nearby ($z < 0.2$) galaxies imaged by the SDSS. A correction factor to the classification fractions measured at the higher redshifts was applied by matching the mean vote fractions of those at the lowest redshift. This technique was valid under the assumption that, within this redhisft range, there would be no cosmological evolution of galaxies, and therefore any change in the mean vote fraction for any morphology with redshift was purely due to this observational bias, and not due to a genuine difference in morphological populations.

In GZH, the redshift range is large enough that cosmological evolution of the morphologies of galaxies is expected, and therefore the previous method of correcting redshift-bias will not work. Instead, we have developed a new method of measuring the change in f_{features} as a function of redshift using a set of simulated FERENGI images of galaxies, described in the next section. These images have been classified by volunteers in Galaxy Zoo in the same way as the GZH sample. This chapter will describe how we measure a correction factor for f_{features} using these data as a function of redshift at fixed surface brightness, and apply the correction to the GZH sample.

4.1.1 The FERENGI code

Describe details of how code articially redshifts images, inputs and outputs, how psf is handled, limitations, handling of surface brightness dimming and k corrections, etc

(Barden et al., 2008)

4.2   The FERENGI sample

To generate an artificially redshifted sample of galaxies to be used in debiasing the Galaxy Zoo: Hubble catalog, a source sample was generated [1] consisting of 288 galaxies from SDSS, all of which were previously classified in GZ2. These galaxies were chosen to span a wide range of morphologies, surface brightnesses, and redshifts. Seven morphological classes were considered: spiral galaxies, edge-on disks without a bulge, edge-on disks with a bulge, face-on disks with a bulge, galaxies with any features, galaxies undergoing mergers, and barred galaxies. For each of these categories, galaxies were chosen with from three "strength" bins, defined using the GZ2 vote fractions. Weak strengths were defined as having $f_{class} < 0.2$, intermediate as $0.2 < f_{class} < 0.8$, and strong as $f_{class} > 0.8$. In each strength bin, galaxies were also chosen to represent three different surface brightnesses: $\mu_r > 21.5$, $20.5 < \mu_r < 21.5$, and $\mu_r < 20.5$. Finally, from each morphological class, strength, and surface brightness bin, one galaxy was chosen for four redshift bins: $z < 0.013$, $0.013 < z < 0.02$, $0.02 < z < 0.025$, and $z > 0.025$, with the exception of the bar class, in which two galaxies were chosen for each redshift bin, doubling the sample size for that class.

The 288 SDSS galaxies were processed with the FERENGI code to mimic *HST* imaging parameters [2] , in order to ultimately measure and correct any redshift-dependant biases in the classifications of the real *HST* images. I-814 and V-606 images, chosen to match the *HST* ACS AEGIS imaging, were output for each subject at a range of redshifts and with a range of applied evolution factors. The range of simulated redshifts possible for any galaxy is dependent on the intrinsic redshift and size of the source galaxy, since the simulated images cannot be resampled at better angular resolution than the original SDSS data. This imposes a minimum simulated "target" redshift that can be achieved for each galaxy. For the lowest redshift bin in the source sample ($z < 0.013$), galaxies could be redshifted the full range of $0.3 < z < 1.0$, in increments of $dz = 0.1$. For the second lowest redshift bin, galaxies could only be redshifted

---

[1]   The source sample for FERENGI was created by the Galaxy Zoo science team in 2012.
[2]   This work was done by Edmond Cheung, a Galaxy Zoo science team member.

in the range $0.5 < z < 1.0$, for the third, galaxies could be redshifted in the range $0.8 < z < 1.0$, and for the highest redshift bin, galaxies were only redshifted in FERENGI to $z = 1.0$. Only galaxies which were redshifted the full range were considered in the debiasing procedure outlined in the next section (4.3.1), because the method calibrates galaxies to a low redshift of $z = 0.3$, data for which is not available for galaxies in the remaining three redshift bins. Last, for each simulated redshift, a range of evolution factors was applied from $0 < e < 3$ in increments of $de = 0.5$.

The final FERENGI sample totals 6,624 simulated images which were classified as part of GZ4, using the same decision tree as used in GZH. The debiasing technique described next (Section 4.3) used only the 4,446 images corresponding to the 72 galaxies which were redshifted the full $0.3 < z < 1.0$ range. Because the debiasing method takes into account surface brightness as a parameter, photometry was measured for all images using SExtractor [3] . The mean surface brighness μ within effective radius (R_e) was calculated as:

$$\mu = m + 2.5 * \log_{10} \left(2 \times (b/a) \times \pi R_e^2\right) \tag{4.1}$$

where m is MAG_AUTO in the I_{814W} band, (b/a) is the galaxy ellipticity (the profile RMS along the semi-major and -minor axes), and R_e is the 50% FLUX_RADIUS converted into arcsec.

4.3 Measuring the drop in f_{features} as a function of z and μ using FERENGI data

4.3.1 Identifying "correctable" and "lower limit" samples.

The objective is to use the simulated data from FERENGI to predict, for a galaxy imaged at a redshift z, and with a measured $f_{\text{features},z}$ value, what its f_{features} value *would have been* if it had been viewed at $z = 0.3$. This predicted value is defined as the "debiased' vote fraction $f_{\text{features,debiased}}$, and is calculated by applying a correction to the measured value of f_{features}.

---

[3] SExtractor measurements for the original FERENGI sample were done by Tom Melvin, a former Galaxy Zoo science team member.
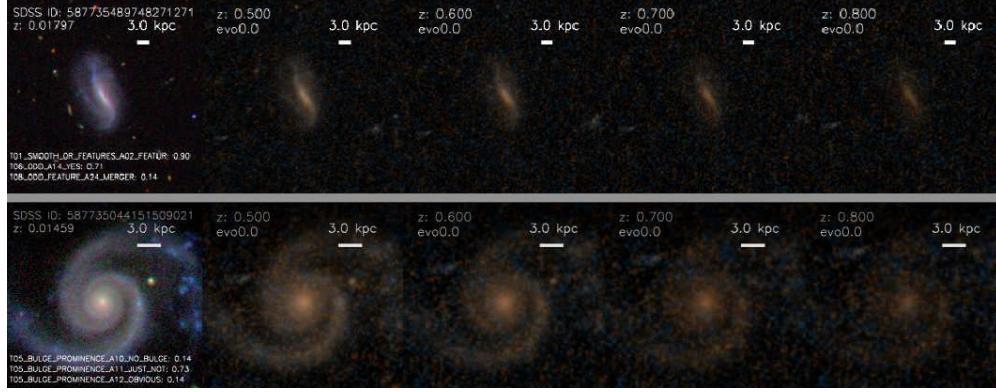
Figure 4.1 Examples of two SDSS galaxies which have been run through the FERENGI code to produce simulated *HST* images. The measured value of f_{features} from GZH for the images in each panel are (1) Top row: $f_{\text{features}} = (0.900, 0.625, 0.350, 0.350, 0.225)$ and (2) Bottom row: $f_{\text{features}} = (1.000, 0.875, 0.875, 0.625, 0.375)$.

The amount that a galaxy's f_{features} vote fraction must be corrected is assumed to primarily depend on the apparent size and brightness of the galaxy. As described in 4.1, these factors will affect the overall clarity of the image viewed by the GZ volunteers, which in turn affects the likelihood of being able to identify distinct feature. The apparent size and brightness are controlled by both instrinsic parameters (absolute size and luminosity), and extrinsic (distance to the galaxy). The change in f_{features} then is measured as a function of redshift (z, an extrinsic freature, measuring distance to the galaxy), and surface brightness (μ, an intrinsic feature, taking into account both brightness and size).

Figure 4.2 shows the change in f_{features} for FERENGI galaxies in bins of redshift and surface brightness. Points in each z, μ represent individual FERENGI galaxies. On the x-axis of each bin is the value of f_{features} measured in that galaxy's $z = 0.3$ image (the lowest redshift of the simulated images). On the y-axis of each bin is the value of f_{features} measured in that galaxy's $z = z$ image, where z corresponds to the redshift associated with that bin. As predicted, the value of f_{features} measured at a higher redshift, z, is, in general, *lower* than the value measured at lower redshift, $z = 0.3$, *for the same galaxy*. This effect is strongest as redshift increases (to the right in Figure 4.2) and as surface brightness decreases (upwards in Figure 4.2).

A reliable predicted value can be obtained so long as the relationship between
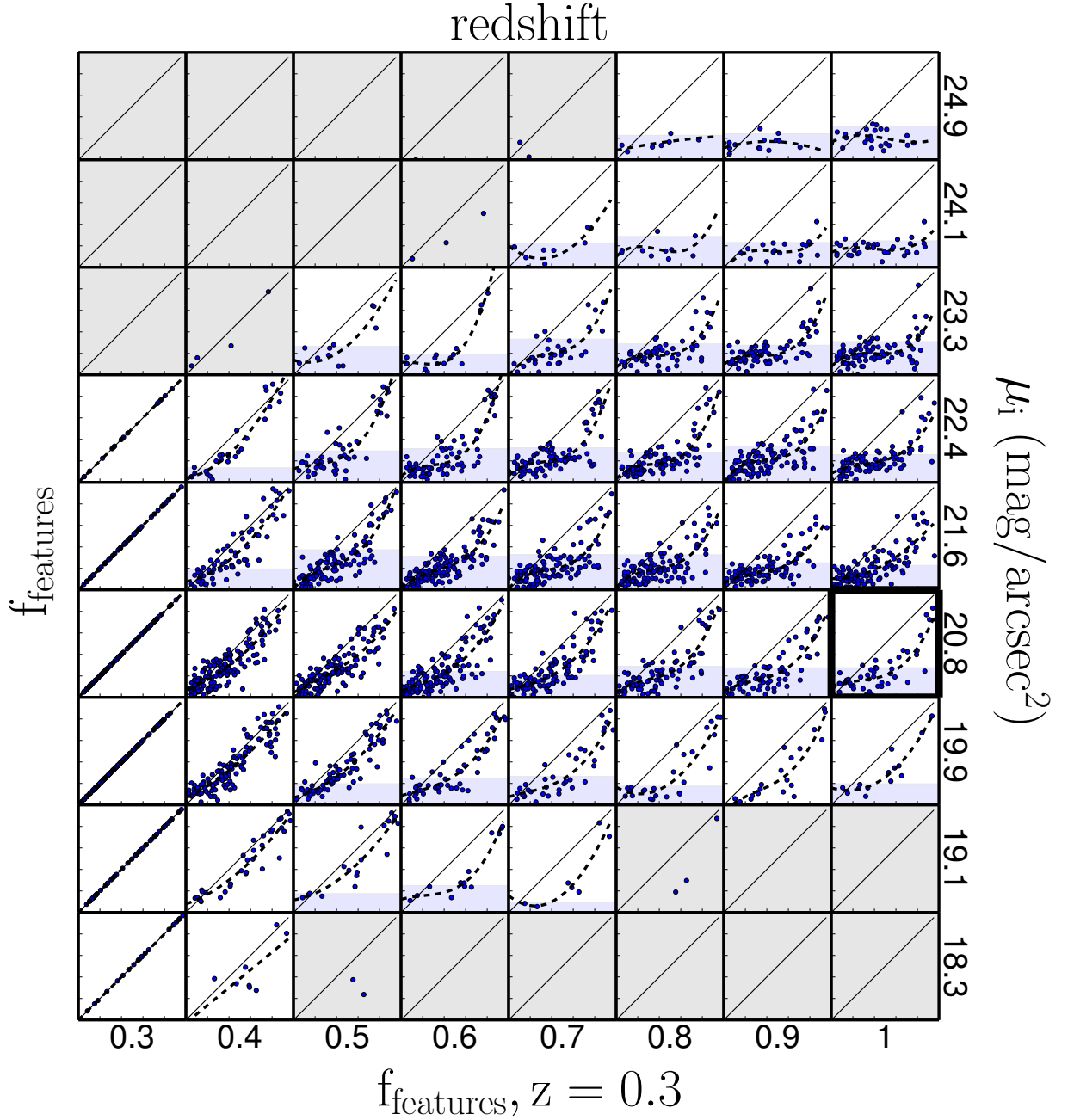
Figure 4.2 Effects of redshift bias in 3,449 images in the FERENGI sample. Each point *in a given redshift and surface brightness bin* represents a unique galaxy. On the *y*-axis in each bin is the f_{features} value of the image of that galaxy redshifted to the value corresponding to that redshift bin. On the *x*-axis is the f_{features} value of the image of the same galaxy redshifted to $z = 0.3$. The dashed black lines represent the best-fit polynomials to the data in each square. The solid black line represents $f_{\mathrm{features},z} = f_{\mathrm{features},z=0.3}$. Regions in which there is a single-valued relationship between f_{features} at high redshift and at $z = 0.3$ are white; those in which there is not are blue, and those with not enough data ($N < 5$) are grey. A larger version of the bin outlined at $z = 1.0$ and $20.3 < \mu < 21.0$ (mag/arcsec^2) is shown in Figure 4.3.
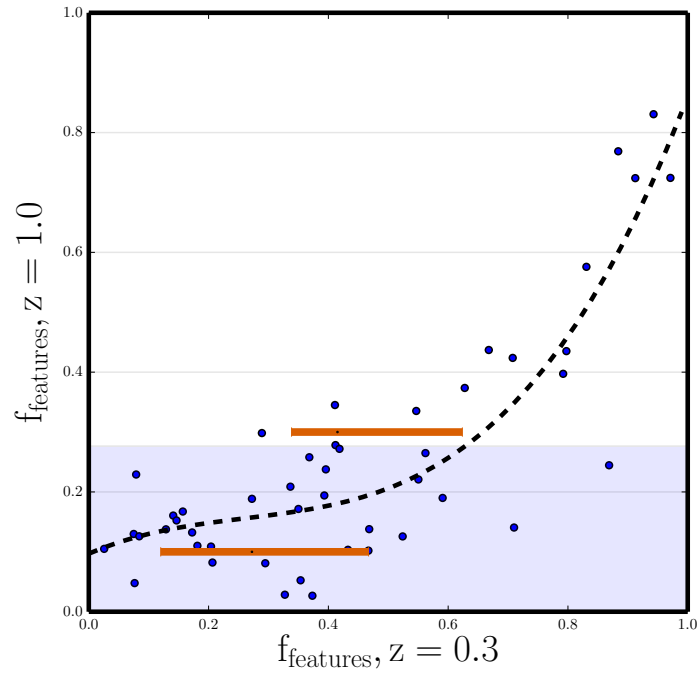
Figure 4.3 A larger version of the dark-outlined square in Figure 4.2, containing FERENGI galaxies that have been artificially redshifted to $z = 1.0$ and have surface brightnesses between $20.3 < \mu < 21.0$ (mag/arcsec^2). The orange bars represent the inner 68% (1σ) of the uncorrectable f_{features} quantiles, which are used to compute the limits on the range of debiased values.

$f_{\text{features},z}$ and $f_{\text{features},z=0.3}$ is single-valued; that is, for a given $f_{\text{features},z}$, there is exactly one corresponding value of f_{features} at $z = 0.3$. Unfortunately, this is *not* always the case. Figure 4.3 shows f_{features} measured at $z = 1$ vs f_{features} measured at $z = 0.3$ for FERENGI galaxies with average surface brightnesses $< \mu >= 20.8$ (a zoomed-in version of the dark outlined bin in Figure 4.2). This figure shows that if the value of f_{features} measured for a galaxy at $z = 1$ is particularly low, there is a wide range that f_{features} could have been if measured at $z = 0.3$. Therefore, a low measured value of f_{features} at high redshift could represent two morphological types of galaxies: 1) The galaxy has no distinguishable features and may be classified as a smooth elliptical, or 2) the galaxy *does* have features, but these have become blurred and too difficult to detect at high redshift.

It is important to identify such regions of surface brightness/redshift/f_{features} space since vote fractions cannot be confidently corrected to a single value for galaxies in these regions. The criteria for determining whether a region of this space is single-valued, and therefore correctable, is as follows: In each surface brightness and redshift bin, the relationship between $f_{\text{features},z}$ and $f_{\text{features},z=0.3}$ is modelled by fitting the data with polynomials of degress n=3,2, and 1, and using the best formal fit out of the three as measured by the sum of the residuals. These fits are shown as the dashed black lines in Figures 4.2 and 4.3. Flat regions of the bins are areas in which there is *not* a clear single-valued relationship between $f_{\text{features},z}$ and $f_{\text{features},z=0.3}$. This is quantified by measuring the slope of the best-fit polynomial to the vote fractions; regions of the bins with a slope less than 0.4 are considered *not* one-to-one, and therefore $f_{\text{features},z}$ cannot be boosted to its $f_{\text{features},z=0.3}$ value. These are colored blue in Figure 4.2 and are referred to as the *lower limit* sample, because the most stringent correction available is that the weighted f_{features} is a lower limit to the true value.

The unshaded regions of Figure4.3 define descrete ranges of redshift, surface brightness, and f_{features} within which a galaxy must lie in order for the debiased vote fraction to be confidently applied. While the appropriate correctable regions were defined as discrete bins, the true correctable region is assumed to be a smooth function of z, μ, and f_{features}. To define this smooth space, a convex hull was calculated to enclose the correctable and lower-limit FERENGI galaxies in the $z - \mu - f_{\text{features}}$ space (see Figure 4.4). The space defined by this hull was used to ultimately separate the GZH galaxies into

Table 4.1 Number of correctable galaxies for the top-level task in GZH, split by *HST* survey.

	Correction type	AEGIS	COSMOS	GEMS	GOODS-N 5-epoch	GOODS 5-epo
correctable	0	2,908	21,169	2,802	1,459	1,1
lower-limit	1	833	5,169	1,021	1,377	1,2
no correction needed ($z \leq 0.3$)	2	955	10,870	1,175	415	4
not enough information (NEI)	3	2,677	43,058	3,559	2,077	2,1
no redshift information	4	1,134	4,688	530	687	1
total		8,507	84,954	9,087	6,015	5,1

correctable samples (those for which a correction to f_{features} can confidently be applied, see next section) and lower-limit samples (those for which a single-valued correction cannot be applied). The final categorization of the GZH sample, split by imaging survey, is shown in Table 4.1.

For the "lower limit" galaxies, since a single debiased f_{features} value cannot be confidently assigned, a *range* of debiased values is estimated. In each z, μ bin in Figure 4.2, the spread of intrinsic values of $f_{\text{features},z=0.3}$ for five quantiles of observed f_{features} is computed - these are denoted by the gray lines in the close-up Figure 4.3. The range of intrinsic values of f_{features} is defined by the upper and lower 1 σ limits, enclosing the inner 68% of the data; this is represented by the orange bars in Figure 4.3. For any galaxy which cannot be directly debiased, these ranges are used to denote the upper and lower limits on the expected values $f_{\text{features},z=0.3}$ as a function of the observed f_{features}.

4.3.2 Computing debiased f_{features} for the "correctable" sample using the ζ equation

For the "correctable" sample of simulated FERENGI galaxies, an equation is derived to model the dropoff in f_{features} with redshift for each galaxy. Such a model is assumed to have the following criteria: (1) For a given galaxy, f_{features} should decrease relative to its $f_{\text{features},z=0.3}$ as redshift increases. (2) The corrected f_{features} value must be contained within 0 and 1, since it is a fraction. (3) The degree of dropoff may depend on the surface brightness of the galaxy. Given these three assumptions, a simple exponential function was derived:
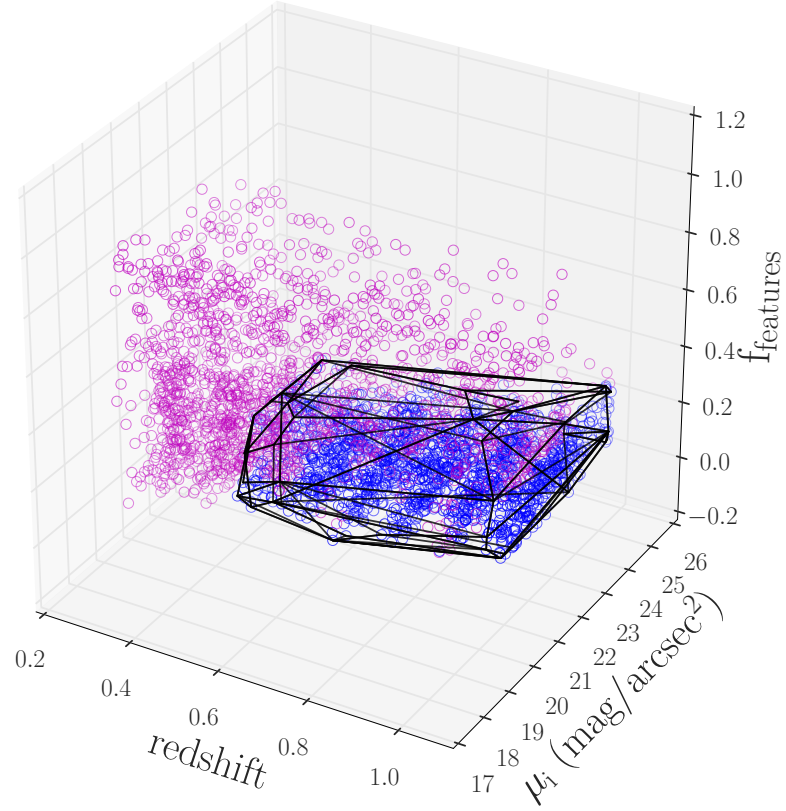
Figure 4.4 The final separation of the correctable and lower-limit samples in red-shift/surface brightness/f_{features} space.**Pink** points are all FERENGI galaxies in the **un-shaded** regions of Figure 4.2. **Blue** points are all FERENGI galaxies in the **blue shaded** regions of Figure 4.2. The solid black line is the convex hull which encloses the uncorrectable points and defines the region of the lower-limit sample.

$$f_{\mu,z} = 1 - (1 - f_{\mu,z=0.3})e^{\frac{z-z_0}{\zeta}} \tag{4.2}$$

where $f_{\mu,z=0.3}$ is the vote fraction at the lowest redshift in the artificially-redshifted FERENGI sample ($z_0 = 0.3$). ζ is a parameter that controls the rate at which f_{features} decreases with redshift.

Equation 4.2 is then fit to each galaxy in the "correctable" FERENGI sample, and ζ is measured for each. Figure 4.5 shows the best fit equations for 16 galaxies, and the ζ corresponding to the best fit is displayed with each galaxy. As it was assumed that surface brightness likely plays a role in the level of dropoff in f_{features}, and hence the value of ζ which controls this dropoff, it is assumed that ζ follows a simple linear dependence with surface brightness:

$$\log_{10}(\hat{\zeta}) = \zeta_0 + (\zeta_1 \times \mu), \tag{4.3}$$

where $\hat{\zeta}$ is the correction factor applied to each galaxy. Figure 4.6 shows the relationship between the derived ζ values and the surface brightness μ of the FERENGI galaxies, which is fit with equation 4.3. The best-fit parameters to this linear fit from least-squares optimization are $\zeta_0 = 0.50$, $\zeta_1 = -0.03$. Interestingly, only a very weak surface brightness dependence is detected. It is difficult to determine from these data whether the weak detection is due to a true lack of dependence, or insufficient data (only 28 galaxies had sufficient data to accurately measure ζ).

Using the ζ parameters measured in the FERENGI sample, a final debiased correction equation is derived to correct the f_{features} vote fractions in the HST data:

$$f_{\text{features,debiased}} = 1 - (1 - f_{\text{features,weighted}})e^{\frac{-(z-z_0)}{\zeta}} \tag{4.4}$$

where $f_{\text{features,weighted}}$ is the weighted vote fraction, and $f_{\text{features,debiased}}$ is bounded between $f_{\text{features,weighted}}$ and 1.

4.3.3 Results and the NEI sample: limitations of the ferengi simulated data

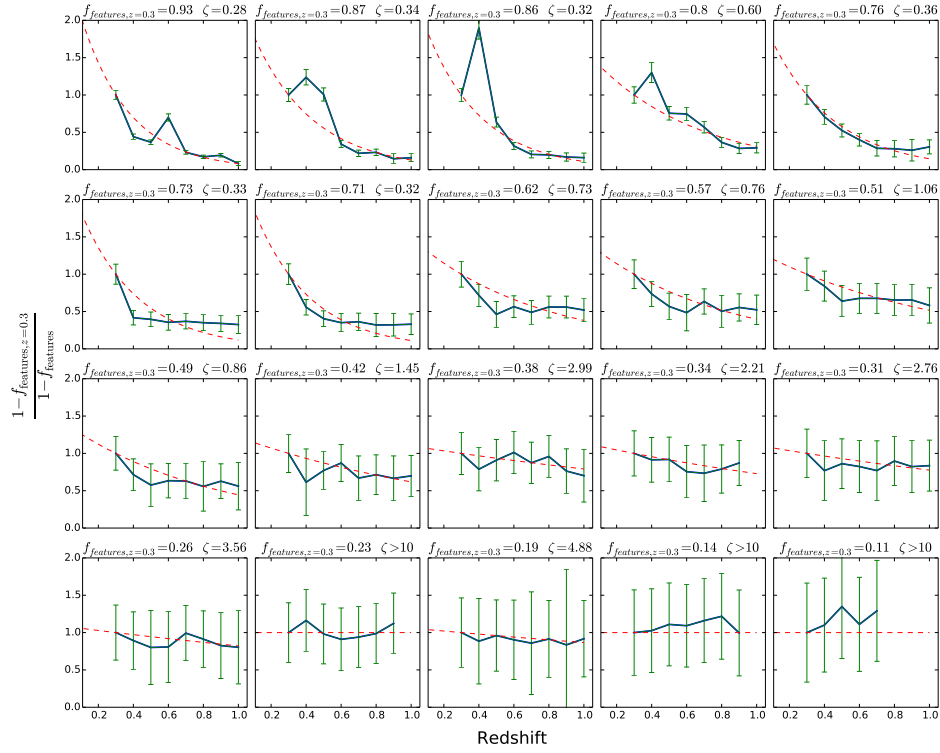- show table of HST sample breakdown 4.1

Figure 4.5 Behaviour of the normalised, weighted vote fractions of features visible in a galaxy (f_{features}) as a function of redshift in the artificial FERENGI images. Galaxies in this plot were randomly selected from a distribution with evolutionary correction $e = 0$ and at least three detectable images in redshift bins of $z \geq 0.3$. The displayed bins are sorted by $f_{\text{features},z=0.3}$, labeled above each plot. Measured vote fractions (blue solid line) are fit with an exponential function (red dashed line; Equation 4.2); the best-fit parameter for ζ is given above each plot.
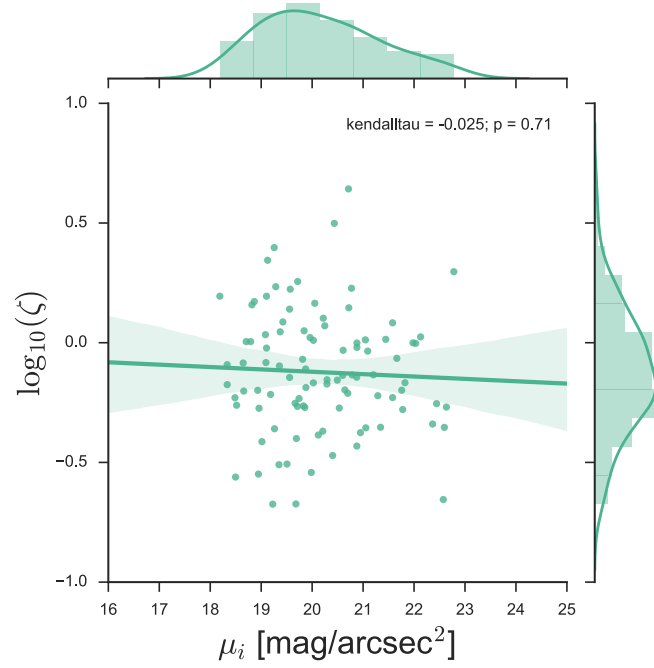
Figure 4.6 All fits for the FERENGI galaxies of the vote fraction dropoff parameter ζ for f_{features} as a function of surface brightness. This includes only the simulated galaxies with a bounded range on the dropoff ($-10 < \zeta < 10$) and sufficient points to fit each function (28 original galaxies, each with varying images artificially redshifted in one to eight bins over a range from $0.3 \lesssim z_{\text{sim}} \lesssim 1.0$).
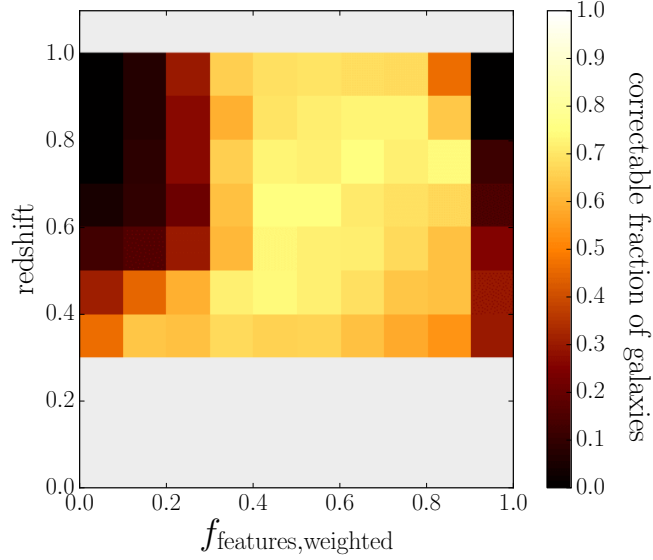
Figure 4.7 Histogram showing the fraction of galaxies that have a finite correction for the debiased vote fractions $f_{\text{features,debiased}}$ as a function of f_{features} and redshift. The parameter space for corrections is limited to $0.3 \leq z \leq 1.0$ due to the sampling of the parent SDSS galaxies and detectability in the FERENGI images.

- show how above method only works for HST galaxies with z/mu corresponding to ferengi space 4.8

- discuss why ferengi can't completely replicate mu distribution of HST (cite Karen response to referee)

- discuss limits shown in 4.7

4.4 Ferengi 2: using simulated images to measure incompleteness in disk fraction as a function of redshift and surface brightness

In the previous section I described how we used the simulated FERENGI images to measure the redshift/surface brightness dependence on f_{features}, and applied the measurements towards a correction factor to the vote fractions directly. In this section I will describe

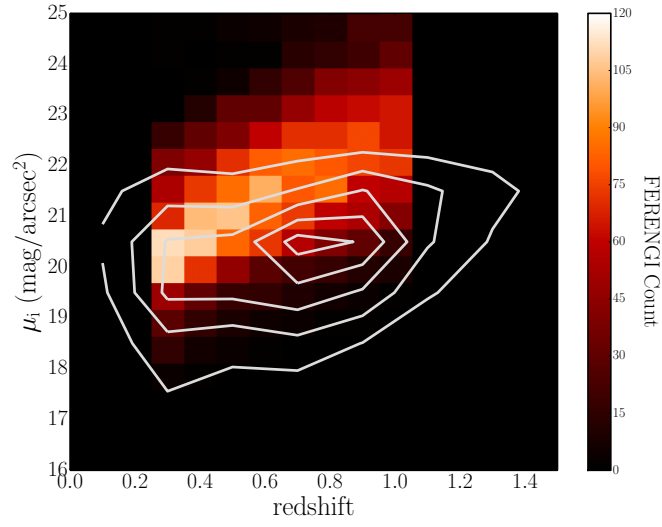Figure 4.8 Surface brightness as a function of redshift for 3,449 FERENGI images and the 102,548 `main` galaxies with measured μ and z values. The colour histogram shows the number of FERENGI images as a function of μ and z_{sim}. White contours show counts for the galaxies in the `main` sample, with the outermost contour starting at $N = 1500$ and separated by intervals of 1500.

the motivation, selection, and application of a second set of FERENGI images used to measure and correct for the incompleteness in *number* of disks detected as a function of redshift and surface brightness, used in the work described in Chapter 5.

4.4.1   The Ferengi 2 Sample

The creation of a second set of FERENGI images was motivated by the scientific goal of measuring the redshift evolution of the fraction of red disk galaxies using the Galaxy Zoo: Hubble dataset. This project is described in full in Chapter 5, but the reasons requiring a new set of simulated images will be described briefly here. First, as described in the previous section, the analysis of the first FERENGI set revealed that, for a large area of z-μ parameter space, galaxies with low measured values of f_{features} could not be corrected to a point that could clearly distingush them as disks with washed-out features or ellipticals. Due to this limitation, any measurement of the number of disk galaxies in a given redshift interval can only be reported as a *lower-limit* to the true value. The difference in the measured lower-limit and the true number of disks is what we will refer to as the *incompleteness* in number of disks detected.

It is possible, then, to use the FERENGI images to measure this incompleteness by measuring the number of disks detected at a given redshift, and comparing to the number of disks detected out of the same galaxies at the lowest redshift (this would be considred the true, or intrinsic, number of disks.) The details of this approach will be described in the next section. A complication specific to this project is that the number of disks will be ultimitely used to compute the *red disk fraction*, that is, the ratio of the number of red disks to all disks, as a function of redshift. It is then necessary to measure the level of incompleteness for both red and blue galaxies separately, to calculate this fraction most accurately.

The color separation method for the *HST* galaxies in Chapter 5 uses NUV, r, and J magnitudes. To separate the FERENGI sample of galaxies into red and blue samples in the same way, these magnitudes are required. In the first set, however, only 44 of the 288 galaxies had these data available, which were not enough to properly measure any incompleteness, especially after binning the data further in surface brightness and redshift. So, a larger set of galaxies to be artificially redshifted, all which had the aforementioned data necessary to separate by color, was required.

This set of new galaxies to be put through the FERENGI code, hereafter refered to as the FERENGI 2 sample, was selected as follows: All candidates were pulled from a parent sample of all SDSS galaxies which had previously been classified in GZ2. As discussed in Section 4.2, only galaxies with redshifts below $z < 0.013$ were able to be redshifted the full simulated redshift range $0.3 < z < 1.0$, so a redshift cut was implemented of $z < 0.013$. These galaxies were cross-matched with catalogs from GALEX (Martin et al., 2005) for NUV magnitudes and 2MASS (Skrutskie et al., 2006) for J magnitudes. 1,435 galaxies fit these criteria.

Bulk SDSS u, g, r, i, and z-band fits images were then downloaded for all 1,435 galaxy candidates [4]. Cutouts were made for each galaxy, using the 90% r-band petrosian radius to set the size of the cutout (PETROR90_R). The default prescription used was to define the edges as 2.5*PETROR90_R, measured from the galaxy as the center. If the galaxy was within this distance from the edge of the bulk fits image, 2.0*PETROR90_R was used. Cutouts were not made for galaxies within this distance from the edge, both to ensure the full galaxy was visible in all cutouts in the sample, and to avoid over-zooming the image. 187 galaxies were thus removed from FERENGI2; an example of such a galaxy "too close" to the edge of the edge is shown in Figure 4.9.

While all 78 $z < 0.013$ galaxies from the original FERENGI sample were successfuly simulated to a minimum redshift of $z_{sim} = 0.3$, this was not always true for the FERENGI2 candidates. Redshift of the source galaxy is the largest factor in determining the minimum possible simulated redshift, but other factors including the size of the psf and physical size of the source galaxy also come into play. All 1,248 candidates were then put through FERENGI at only the lowest redshift $z_{sim} = 0.3$ to begin, and each image was visualy inspected to determine whether the code succeeded. 312 "failures" were detected; two examples are shown in Figure 4.10. The remaining 936 "successes" were then artificially redshift the full range of $0.3 < z < 1.0$ in increments of $dz = 0.1$; these make up the final FERENGI2 sample of 7,488 images of 936 galaxies redshifted 8 times. A single evolution factor, rather than a range, of $e = 1$ was applied to all images. This value was chosen by analyzing the spectra template models of Brinchmann et al. (2004), which showed that the most typical galaxies evolve in brightness by one magnitude per redshift. Example images are shown in Figure 4.11
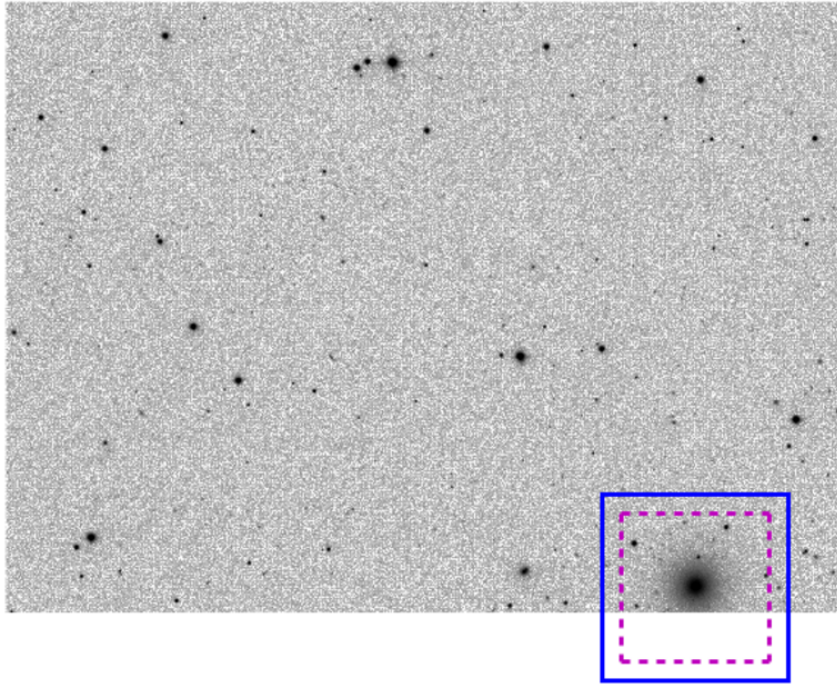
---

[4] http://data.sdss3.org/bulkFields

Figure 4.9 Example of a galaxy overlapping the edge of the SDSS frame. Shown is the bulk r-band fits image for SDSS DR12 run 3903, camcol 6, and field 60. The boxed-in galaxy (SDSS DR12 objid 1237662239079268544) is too close to the edge of the image to create a cutout that encloses the entire galaxy. The pink dashed box indicates a cutout size of 2*petroR90_r, the blue solid line indicates a cutout size of 2.5*petroR90_r.
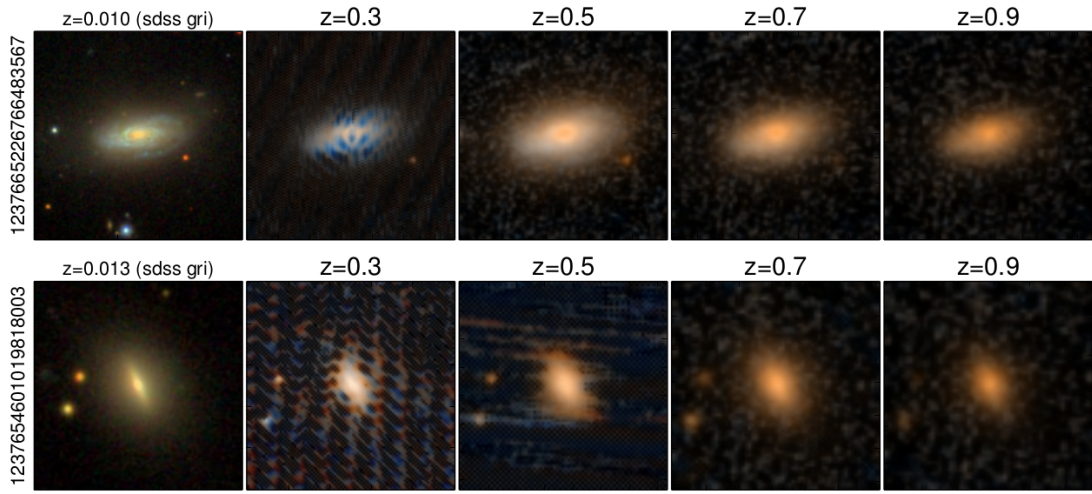
Figure 4.10 Examples of two galaxies whose minimum simulated redshifts in FERENGI were larger than $z_{sim} = 0.3$. These were detected via visual inspection and removed from the final FERENGI2 sample.
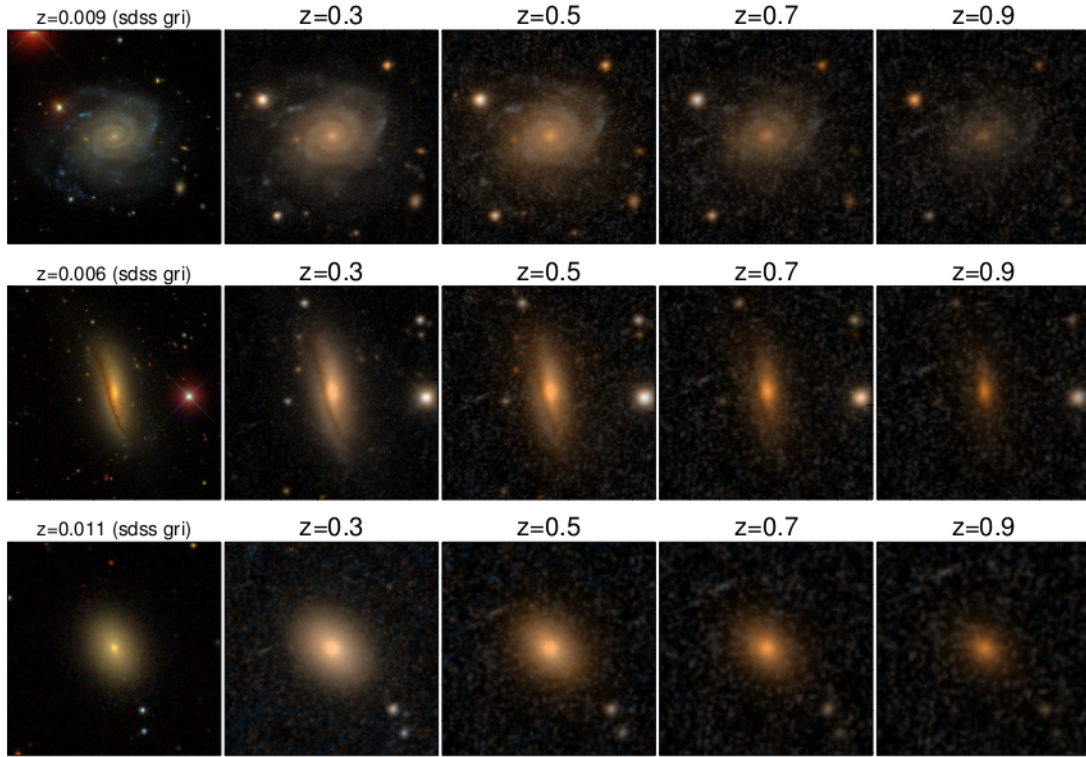
Figure 4.11 Examples of FERENGI2 galaxies. The left is the original gri-composite image of the source galaxy. Images on the right are simulated output from the FERENGI code. Only four of the eight simulated redshifts are shown in the interest of space.

Chapter 5

GZH red disk fraction

red disk fraction project

Chapter 6

Summary & Future Work

References

Barden, M., Jahnke, K., & Häußler, B. 2008, The Astrophysical Journal Supplement Series, 175, 105

Brinchmann, J., Charlot, S., White, S. D. M., et al. 2004, Monthly Notices of the Royal Astronomical Society, 351, 1151

Martin, D. C., Fanson, J., Schiminovich, D., et al. 2005, The Astrophysical Journal, 619, L1

Muzahid, S., Kacprzak, G. G., Churchil, C. W., et al. 2015, 15

Skrutskie, M. F., Cutri, R. M., Stiening, R., et al. 2006, The Astronomical Journal, 131, 1163